GAO, Dian-ce, et al. A model-based adaptive method for evaluating the energy impact of low delta-T syndrome in complex HVAC systems using support vector regression. Building Services Engineering Research and Technology, 2016, 37.5: 573-596.

**This is the Pre-Published Version.**

This is the accepted version of the publication Gao, D. C., Wang, S., Gang, W., & Xiao, F. (2016). A model-based adaptive method for evaluating the energy impact of low delta-T syndrome in complex HVAC systems using support vector regression. Building Services Engineering Research and Technology, 37(5), 573-596.  DOI: 10.1177/0143624416640760.

# A Model-based Adaptive Method for Evaluating The Energy Impact of Low Delta-T Syndrome In Complex HVAC Systems Using Support Vector Regression

Dian-ce Gao, Shengwei Wang*, Wenjie Gang and Fu Xiao

Department of Building Services Engineering,

The Hong Kong Polytechnic University, Kowloon, Hong Kong

* Corresponding author. +852 27665858; fax: +852 2774 6146.

*E-mail address*: beswwang@polyu.edu.hk

## Abstract

Low delta-T syndrome refers to the situation where the measured differential temperature of the overall terminal air-handling units is much lower than the normal value expected. It widely exists in the existing HVAC systems and results in increased energy consumption. This paper presents a model-based method to evaluate the energy impact on the chilled water pumps due to the low delta-T syndrome in a complex chilled water system. When the low delta-T syndrome occurs, the chilled water pumps would deviate from their normal working conditions with increased power consumption. Models are developed to predict the reference benchmarks of the chilled water pump power based on the current cooling load, control rules and preset set-points. The energy impact on the chilled water pumps can be determined by comparing the measured current pump power with the predicted benchmark. Support Vector Regression (SVR) method is introduced for predicting the chilled water flow rate of the overall terminal units. Adaptive concept is employed to enhance the prediction accuracy of the overall pressure drop of the hydraulic water network under various working conditions. The proposed method is tested and validated in a dynamic simulation platform built based on a real complex HVAC system. Results show that the proposed method can accurately evaluate the impact of the low delta-T syndrome on energy consumption of the chilled water pumps.

***KEYWORDS:*** *Chilled water system; low delta-T syndrome; building energy; model-based adaptive method*

## Practical Application

Low delta-T syndrome widely exists in existing HVAC systems and results in increased energy consumption. This paper presents a model-based method for practical applications in assessing the energy impact on the chilled water pumps due to the low delta-T syndrome in a complex chilled water system. When the low delta-T syndrome occurs in a system, this method can be used to predict the reference benchmark of energy use of chilled water pumps based on the measured cooling load profiles, the control rules used and the preset set-points. The energy impact can be determined by comparing the measured actual energy consumption with the predicted benchmark. The evaluation results could help the operators to conveniently monitor the energy performance of the chilled water distribution system as well as to judge whether or not taking measures to identify and correct the related faults that result in the low delta-T syndrome.

## Nomenclature

| | |
|---|---|
| *AHU* | air handling unit |
| $b_0$–$b_1$ | coefficients |
| $c_0$–$c_2$ | coefficients |
| $d_0$–$d_2$ | coefficients |
| $e_0$–$e_1$ | coefficient |
| $f_0$–$f_3$ | coefficient |
| *Fre* | frequency (Hz) |
| *H* | pump head (kPa) |
| *M* | water mass flow rate (kg/s) |
| *N* | number |
| *NTU* | number of transfer units |
| *P* | power consumption (kW) |
| *PCHWP* | primary chilled water pump |
| *PD* | pressure difference |
| *Q* | cooling load (kW) |
| *Rat* | ratio |
| *S* | flow resistance (kPa/(kg/s)$^2$) |
| *SCHWP* | second chilled water pump |
| *SG* | specific gravity of the fluid being pumped |
| *T* | temperature (°C) |
| *UA* | conductance-area product (W/K) |
| **Greek symbols** | |
| $\eta$ | efficiency |
| **Subscripts** | |
| *a* | air |
| *ahx* | after heat exchanger |
| *bhx* | before heat exchanger |
| *des* | design |
| *fic* | fictitious |
| *hx* | heat exchanger |
| *in* | inlet |
| *indoor* | indoor |
| *m* | motor |
| *pf* | pump fitting |
| *pipe* | pipeline |
| *pri* | primary side |
| *pu* | pump |
| *sec* | secondary side |
| *term* | terminal loop |
| *tot* | total |
| *vfd* | variable frequency drive |
| *w* | water |
| *zone* | zone |
| **Superscripts** | |
| * | benchmark |
| *k* | numbering of time step |

## 1. Introduction

Heating, ventilating and air-conditioning (HVAC) systems are the major energy consumers in the commercial buildings. According to the statistical data, nearly 47% of building energy was consumed by space heating and cooling in U.S [1]. During the last two decades, considerable efforts have been made to enhance the energy performance of buildings and building HVAC systems [2-10].

Currently, the primary-secondary chilled water systems still dominate in the existing commercial buildings. A typical primary-secondary chilled water distribution system consists of two loops: the primary loop with constant flow and the secondary loop with variable flow. A bypass pipeline decouples the two loops. Since the cooling coils of the Air-Handling Units (AHUs) are selected to produce a temperature rise at full load that is equal to the temperature differential selected for the chillers. The flow rate of secondary loop should be therefore equal to that of the primary loop under full load condition and should be less than that of primary loop under part load conditions.

While in real applications, most of the primary-secondary systems do not work efficiently as expected due to the low delta-T syndrome. Low delta-T syndrome refers to the situation where the mean water temperature difference produced by the overall AHUs is much lower than its normal value expected. When a serious low delta-T syndrome occurs, the chilled water circulated in the secondary loop is significantly over-supplied when compared to the normal demand. Once the secondary loop water flow rate exceeds that of the primary loop, the water flow in the bypass line would flow in a reverse direction (i.e. from return side to supply side), which is also called the deficit flow. The deficit flow problem and low delta-T syndrome may cause a series of operational problems, such as the high supply water temperature to terminal units, the over-supplied chilled water and the increased energy consumption of the secondary pumps.

The low delta-T syndrome is one of the serious operation problems degrading the building energy performance, which was frequently studied in the last two decades [11-14]. Kirsner [11] pointed out that the low delta-T chilled water plant syndrome exists in almost all large

distributed chilled water systems. Many possible reasons of the deficit flow problems have been studied [15-18]. Taylor [16] stated that some causes can be avoided through careful calibrations and commissioning, such as improper set-point or controls calibration, the use of three-way valves, improper coil and control valve selection, no control valve interlock, and uncontrolled process load, etc.. While some causes cannot be avoided, such as reduced coil effectiveness, outdoor air economizers and 100% outdoor air systems.

Some studies focused on dealing with the low delta-T syndrome and deficit flow problem [11, 19-22]. Fiorino [21] indicated strongly that a higher delta-T could be achieved by proper application of cooling coils, controls systems, distribution pumps, and piping systems. Up to 25 practical methods were recommended to achieve high chilled water delta-T covering component selection, sensor calibration, and configurations of distribution systems, etc. Gao [22] presented a fault-tolerant control strategy for the secondary chilled water pumps to solve the low delta-T problem. Kirsner [13] analyzed the advantage the use of check valve in the bypass line and thought that installing check valve in the bypass line is a cheap and a simple improvement to primary-secondary design of chilled water plants that allows a plant to deal with low delta-T syndrome. Wang [23] presented an approach that experimentally validated the feasibility of using a check valve in the chilled water bypass line to solve the low delta-T syndrome.

In a real HVAC system suffering from the low delta-T syndrome, it is essential to estimate how much energy is wasted. The accurate estimation of energy impact could be necessary for the decision-making on whether or not taking measures to correct the related faults. Some existing practical methods have been used to evaluate the energy impact due to the low delta-T syndrome in practical applications [14,16]. The main principle of the exiting evaluation method is to simply compare the energy consumption of the system with faults with the historic data without faults. The existing method could be simple for field implementations but could be not accurate enough if the cooling load profiles during the two periods are significantly different. Actually, it is very hard to obtain adequate fault-free historical operation data, which covers the wide range of all possible working conditions and cooling load profiles of the HVAC system. The HVAC system is a typical non-linear system.

Although the total cooling load profile is the same in two days, the energy consumption of the secondary pumps is still possible not to be the same in the two days. Due to the high nonlinearity, the total chilled water demand is not proportional to the total cooling load handled by all the AHUs. For a system involving multiple AHUs, when handling the same total cooling load, the total chilled water demand will be significantly different when the cooling load distribution profile for each AHU changes.

Since there is still lack of effective methods for quantitatively evaluating the energy impact of chilled water pumps due to the low delta-T syndrome, this paper therefore presents a model-based method for practical implementations based on the measured operation data. When the low delta-T syndrome occurs in a system, this method can predict the benchmark of the chilled water pump energy consumption based on the current cooling load, control rules and preset set-points. The benchmark here means the normal energy consumed by the overall chilled water pumps under the current cooling load if there is no low delta-T syndrome occurring. The energy impact can be determined by comparing the measured actual energy consumption with the predictive benchmark. The scope of this paper focuses on how to evaluate the energy impact when the system suffers from the low delta-T syndrome. The issues concerning the reasons that cause the low delta-T syndrome are not discussed.

Three major innovative works are involved in this study. First, the proposed model-based method can perform the accurate evaluation of the energy impact of the chilled water pumps under various working conditions when the low delta-T syndrome occurs. Second, the Support Vector Regression (SVR) method is employed to enhance the accuracy of the predictive model of the chilled water flow rate considering the time-varying load distribution among individual AHUs. Third, adaptive concepts are adopted to update the parameters of the pressure drop model for the more accurate prediction of the pump head according to the measured operation data. This method is evaluated on a simulated dynamic system constructed based on a real system in a high-rise building in Hong Kong. This method can be used for online or offline evaluation or diagnosis of the performance of the chilled water system when suffering from the low delta-T syndrome in order to avoid excessive energy is wasted.

This paper is organized as follows: Section 2 gives a brief description of the studied building and HVAC system. Section 3 introduces the model-based adaptive method. Section 4 describes the performance tests and evaluation of the proposed method. The last section is the conclusion.

## 2. Building and system descriptions

The central cooling system concerned in this study is a complex primary-secondary chilled water system in a super high-rise building in Hong Kong [24]. The building is about 490 meters high with approximately 321,000 $m^2$ floor areas, consisting of a basement of four floors, a block building of six floors and a tower building of 98 floors. As shown in Fig.1, this central chilled water plant employs six identical constant speed centrifugal chillers to provide chilled water for air handling units in the building. The rated cooling capacity and power consumption of each chiller are 7230 kW and 1270 kW respectively. The design chilled water supply and return temperatures for chillers are 5.5°C and 10.5°C respectively. Each chiller is associated with a constant speed primary chilled water pump. The primary loop is decoupled with the secondary loop through the bypass line. The secondary chilled water system is divided into four zones, in which Zone 2 is supplied with the chilled water from chillers directly. The plate heat exchangers are employed to transfer cooling energy from chillers to terminal air-handling units in Zone 1, Zone 3 and Zone 4 to avoid chilled water pipelines and terminal units from suffering extremely high static pressure. All the secondary pumps are equipped with variable speed drivers and all the primary pumps are constant speed pumps. The specifications of chilled water pumps are listed in Table 1. This central chilled water plant frequently suffered from the deficit flow problem and low delta-T syndrome after its use since the middle of 2008 [18].

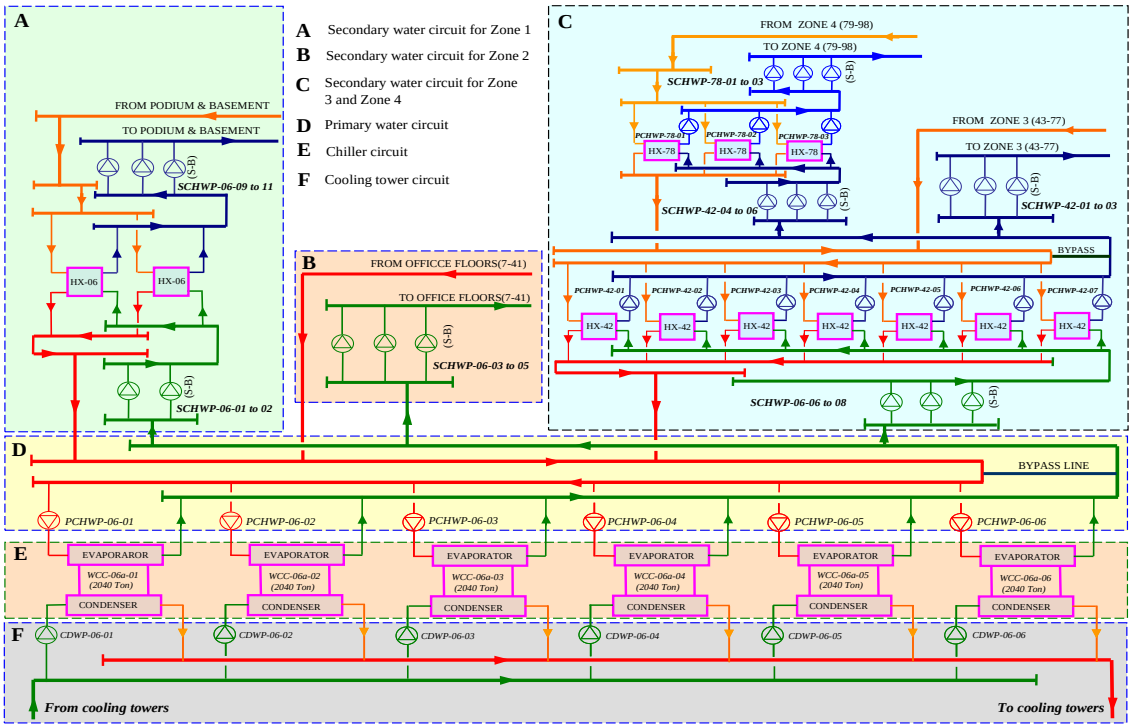


Fig. 1 Schematic of the chilled water system

Table 1 Specifications of chilled water pumps

| Pumps | Number* | Flow ($L/s$) | Head ($kPa$) | Power ($kW$) | Efficiency (%) | Remarks |
|---|---|---|---|---|---|---|
| Primary water pumps | | | | | | |
| PCHWP-06-01 to 06 | 6 | 345 | 310 | 126 | 84.9 | Constant speed |
| Secondary pumps for Zone1 | | | | | | |
| SCHWP-06-01 to 02 | 1(1) | 345 | 241 | 101 | 82.3 | Variable speed |
| SCHWP-06-09 to 11 | 2(1) | 155 | 391 | 76.9 | 78.8 | Variable speed |
| Secondary pumps for Zone 2 | | | | | | |
| SCHWP-06-03 to 05 | 2(1) | 345 | 406 | 163 | 85.9 | Variable speed |
| Pumps for Zone 3 and Zone 4 | | | | | | |
| SCHWP-06-06 to 08 | 2(1) | 345 | 297 | 122 | 84.0 | Variable speed |
| PCHWP-42-01 to 07 | 7 | 149 | 255 | 44.7 | 85.0 | Constant speed |
| SCHWP-42-01 to 03 | 2(1) | 294 | 358 | 120 | 87.7 | Variable speed |
| SCHWP-42-04 to 06 | 2(1) | 227 | 257 | 69.1 | 84.4 | Variable speed |
| PCHWP-78-01 to 03 | 3 | 151 | 202 | 36.1 | 84.5 | Constant speed |
| SCHWP-78-01 to 03 | 2(1) | 227 | 384 | 102 | 85.5 | Variable speed |

*Value in parentheses indicates number of standby pumps

The subsystem of Zone 3 is selected as the example to be studied due to that it is the complicated primary-secondary system involving plate heat exchangers. Such pumping paradigm is normally adopted in the chilled water distribution system in most of actual

high-rise buildings. The simplified schematic of Zone 3 is illustrated in Fig. 2. In this subsystem studied, plate heat exchangers are employed to transfer the cooling energy from the chiller to the terminal AHUs. At the primary side of heat exchangers (i.e., before heat exchangers), variable speed pumps (SCHWP-06-06 to 08) deliver the chilled water from the chillers to the plate heat exchangers. At the secondary side of heat exchangers (i.e., after heat exchangers), each plate heat exchanger is associated with a constant speed pump to ensure the constant flow rate at the secondary side of each heat exchanger. Variable speed pumps (SCHWP-42-01 to 03) are employed to deliver the outlet water from the heat exchangers to the terminal AHUs.

## 3. Formulation of the model-based adaptive method

### 3. 1 Basic analysis of the cooling coil performance

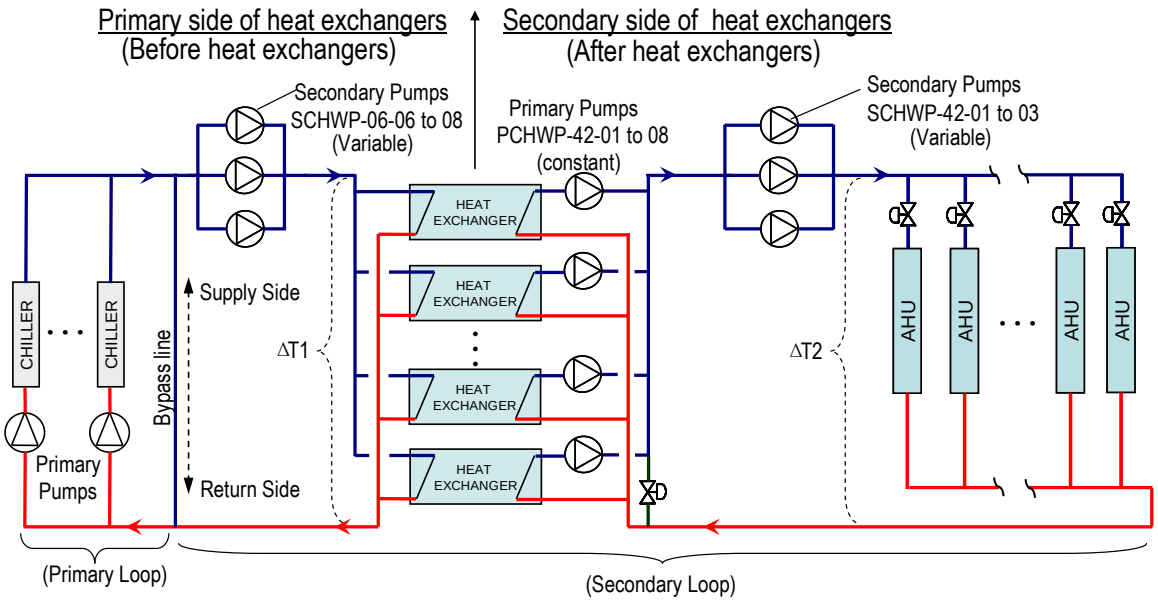


Fig. 2 The simplified schematic of chilled water system of Zone 3

For the studied HVAC system involving plate heat exchangers in the secondary loop, there are two key temperature differences concerned. One is the temperature difference between main inlet and outlet water at the primary side of the plate heat exchangers group (i.e., *ΔT1* in Fig.2), and another one is the temperature difference between the main supply and return water of the overall AHUs (i.e., *ΔT2* in Fig.2).

When the low delta-T syndrome occurs at the primary side of heat exchangers, it means that *ΔT1* is lower than the normal value and the water flow rate through the pumps (SCHWP-06-06 to 08) exceeds the normal value expected. The pump energy consumption thus is increased. If *ΔT1* is extremely low and the water flow rate at the primary side of plate heat exchangers will be significantly increased to be more than that of the primary loop, which will trigger the deficit flow. The water in the bypass line would move from return side to the supply side. The return water would mix with the supply water from the chillers, resulting in increased temperature of the water to the heat exchangers. For the heat exchangers, the high inlet water temperature will further result in more demand for the chilled water at the primary side for the same cooling transfer. The deficit flow will be worsened. Hence, it becomes a vicious circle. Similarly, when the low delta-T syndrome occurs at the secondary side of heat exchangers, *ΔT2* will drop. The water delivered to all AHUs and the energy consumed by the related pumps (SCHWP-42-01 to 03) would be increased.

Simulation studies were conducted to demonstrate how the coil performance of an AHU is degraded by the low delta-T syndrome resulted from a typical fault (i.e., coil fouling). Using the detailed physical model of the cooling coil, some simulations were carried out to study the performance of a cooling coil suffering from the fault (e.g., coil fouling) under different levels. In the simulations, the temperature and humidity of the inlet air as well as the inlet water temperature were fixed, and the water flow rate of the coil was modulated to control the outlet air temperature at a fixed set-point. Fig. 3 shows the test results under various cooling load ratios when the water thermal resistance of tubes increases by 20% and 40%, respectively. Cooling load ratio means the measured cooling load divided by the rated cooling load under the design conditions. Water flow ratio reflects the measured water flow divided by the rated water flow under the design conditions.

As shown in Fig.3, when there are no faults, the chilled water flow rate and the temperature difference (delta T) of a coil are not linear to its cooling load handled. The cooling capacity produced by unit water flow is gradually decreased with the increase in the cooling load ratio. The temperature difference becomes lower with the increase in the cooling load ratio. When

the faults are introduced, the required water is increased and the temperature difference produced becomes lower when handling the same cooling load. The situation becomes serious with the increase in the fault severity. The tests illustrate that the chilled water demand will be highly increased under the low delta-T syndrome. In a chilled water distribution network involving multiple AHUs, it is necessary to detect the healthy status of the system water temperature difference and evaluate the negative impact on the pump energy consumption when the low delta-T syndrome occurs.

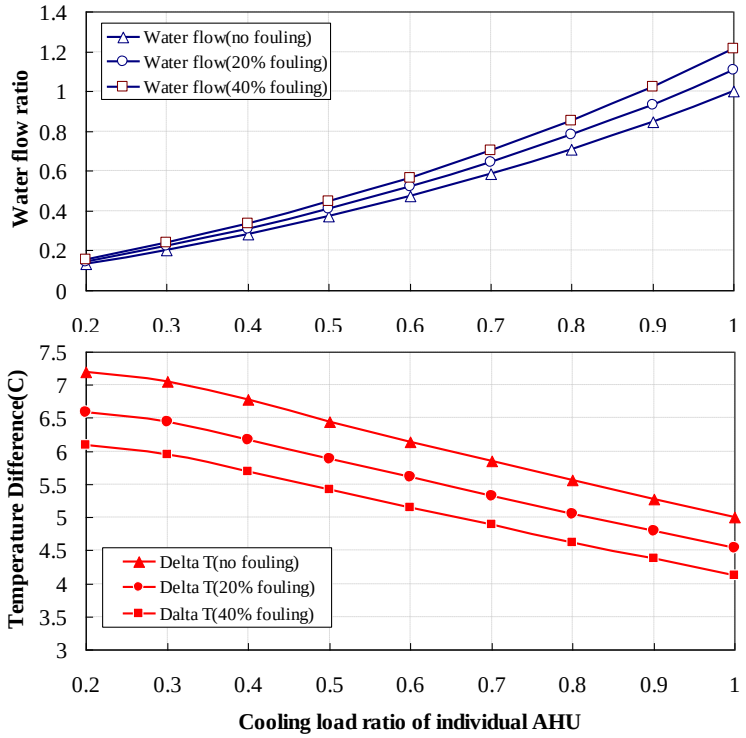


Fig. 3 Performance of a cooling coil suffering from the fault of water fouling

### 3. 2 Basic principle and structure of the proposed method

In this paper, a model-based method is presented to quantitatively assess the energy impact on the chilled water pumps due to the low delta-T syndrome. When the low delta-T syndrome occurs, the system water flow rate, the operating number of heat exchangers/pumps, the hydraulic pressure drop and the pump energy consumption will significantly deviate from their normal levels. Since the indoor thermal comfort can still be maintained at the required level even with the occurrence of the low delta-T syndrome, the actual cooling load can be considered reasonable. The major work of this study is to make the accurate prediction of the

power benchmarks of the overall chilled water pumps under various cooling load conditions when the low delta-T syndrome occurs. The benchmark here means the normal energy consumed by the overall chilled water pumps under the same cooling load conditions without the occurrences of the low delta-T syndrome. When the low delta-T syndrome exists, the energy impact of pumps can be determined by comparing the measured actual power of pumps with the benchmark. However, due to the high nonlinearity of the HVAC system, the main challenges to be addressed include: how to accurately predict the required water flow of all AHUs considering the time-varying cooling load ratios of individual AHUs, and how to accurately predict the pressure drop of the chilled water network under the predicted water flow rate considering the time-varying water resistances of the network. The required sensors (e.g. temperature, water flow, air flow, pressure) and meters (e.g. cooling load meter and power meter) for a complex chilled water system are shown in Fig. 4.

This method mainly consists of four stages, as shown in Fig. 5. At the data processing stage, the data measured from HVAC systems are firstly preprocessed to remove the obviously unreasonable data through outlier removing and data filter. At the water flow prediction stage, under the measured cooling load, the benchmark of the required chilled water flow rate at the secondary side of the heat exchangers ($M^*_{w,AHUs}$) is determined using the global AHU model. The benchmark of the required chilled water at the primary side of the heat exchangers ($M^*_{w,tot,bhx}$) is determined using heat exchanger model. At the power prediction stage, water network models are utilized to predict the benchmarks of pressure drops ($PD^*_{sec,bhx}$ and $PD^*_{sec,ahx}$) of the loop at the primary and secondary sides of heat exchangers respectively. The benchmark of the total energy consumption of pumps ($P^*_{pu,tot}$) is determined using pump models. Lastly, at the energy impact assessment stage, the energy impact ($\Delta P_{pu,tot}$) can be determined by comparing the measured actual energy consumption of the overall chilled water pumps with the predicted benchmark. The detailed descriptions of the models will be described in the following parts.

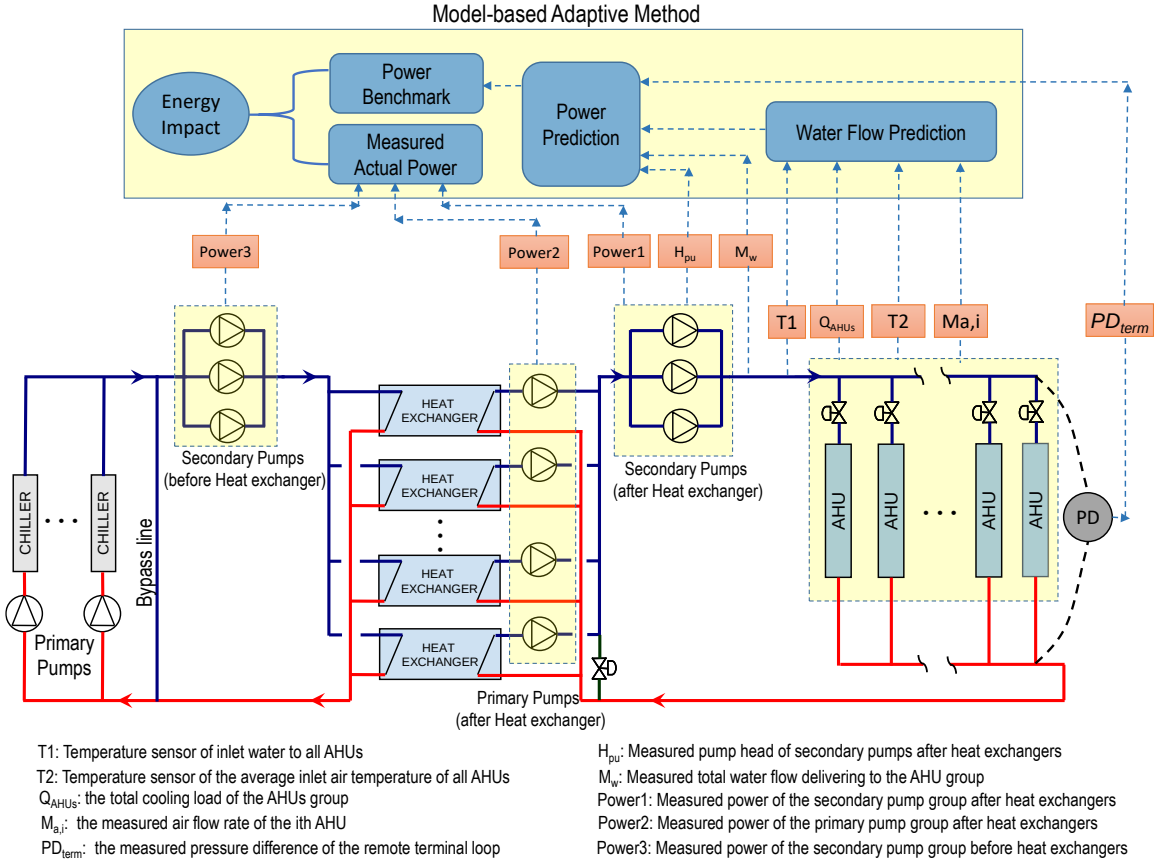


Fig. 4 Schematic of the required sensors and meters for a complex chilled water system

### 3.3 Global AHU model based on SVR method

The global AHU model is developed to predict the benchmark of the total chilled water flow of all AHUs in the zone concerned under the measured cooling load. The studied AHU system is a variable air volume (VAV) system. For each AHU, the supply air temperature is controlled at the preset set-point by modulating the required chilled water flow rate. For the individual AHU, the water flow rate required is strongly dependent on its cooling load, the inlet water temperature and the inlet air temperature. However, for a system involving multiple AHUs, the overall water flow demand of all AHUs would be complex because the cooling load ratio of individual AHU is still a major factor that affects the total chilled water demand. It means that although the total cooling load handled by the overall AHUs is the same, the overall system water flow would be significantly different if the cooling load ratio of individual AHU is different.

For instance, a simulation-based case study was conducted to study the variation of the total chilled water flow rate of a system consisting of two identical AHUs. In the study, the total cooling load handled by the two AHUs was maintained unchanged at all time, and only the cooling load ratio of the individual AHU varied. In the simulations, the temperature and humidity of the inlet air as well as the inlet water temperature were fixed, and the water flow rate of the coil was modulated to control the outlet air temperature at a fixed set-point. From the results as shown in Table 2, when the cooling load of each AHU is the same (Case #1), the total water flow rate is 10.58 kg/s. When the cooling load ratio of AHU-1 is 10% and the cooling load ratio of AHU-2 is 90% (Case #5), the total water flow rate is 12.92 kg/s, which is 22.1% greater than that in Case #1. The test results indicate that the larger difference in the load ratio of the two AHUs, the more total chilled water is required when handling the same total cooling load. Therefore, the load ratio of each AHU is a sensitive variable that affects the total water demand of a chilled water system.

Table 2 Water flow rate variation under various cooling load distributions

| | AHU-1 | | AHU-2 | | Total | | Deviation of total water demand (%) |
|---|---|---|---|---|---|---|---|
| | Water flow rate (kg/s) | Individual load ratio (%) | Water flow rate (kg/s) | Individual load ratio (%) | Water flow rate (kg/s) | System load ratio (%) | |
| Case #1 | 5.29 | 50 | 5.29 | 50 | 10.58 | 50 | - |
| Case #2 | 4.01 | 40 | 6.71 | 60 | 10.72 | 50 | 1.3 |
| Case #3 | 2.88 | 30 | 8.26 | 70 | 11.14 | 50 | 5.3 |
| Case #4 | 1.89 | 20 | 9.98 | 80 | 11.86 | 50 | 12.1 |
| Case #5 | 1.03 | 10 | 11.89 | 90 | 12.92 | 50 | 22.1 |

When studying the performance of AHUs group as a whole, the cooling ratios of individual AHUs were not properly considered in the existing studies [25, 26]. In this study, the global AHU model for the determination of the benchmark of the overall AHU water flow ($M^*_{w,AHUS}$) can be described in Eq.(1), in which the cooling load ratios of individual AHUs (i.e., $Rat_1 \ldots Rat_n$) are considered. Since there is normally no energy meter (or water flow meter) installed for the individual AHUs in most of the real buildings, the cooling load ratio cannot be determined accurately. To address this problem, the measured air flow rate ($M_a$) of each AHU

fan divided by the design value ($M_{a,des}$) can be employed to indicate the load ratio approximately. The air flow rate can be easily determined by the air flow meter.

$$M^{*}_{w,AHUS} = f(Q_{AHUs}, T_{w,in,AHUs}, T_{a,in,AHUs}, Rat_1, \cdots, Rat_n) \quad (1)$$

$$Rat_i = M_{a,i} / M_{a,des,i} \quad (2)$$

where, $Q_{AHUs}$ is the total cooling of the AHUs group. $T_{w,in,AHUs}$ is the inlet water temperature of AHUs. $T_{a,in\ ,AHUs}$ is the average inlet air temperature of all the AHUs. *Rat* is the load ratio of individual AHUs. n is the number of AHUs. $M_a$ is the measured air flow rate. Subscript *i* refers the *i th* AHU.

There is considerable nonlinearity between the water temperature difference and the cooling load for the AHUs. A non-linear approach, the Support Vector Regression (SVR), is adopted for the development of the global AHU model. SVR, developed by Vapnik a decade ago [27, 28], is a machine learning algorithm based on structural risk minimization from statistical learning theory. The basic idea of SVR is to introduce kernel function, map the input space into a high-dimensional feature space by a nonlinear mapping and perform a linear regression in this feature space. SVR has been widely used in the building science regions [29-32] due to the prominent advantages, like excellent properties in learning limited samples, good generalization ability, etc.

The SVR can be briefly introduced as follows according to [27, 28]. Given a training set of pairs ($x_i$, $y_i$), i=1…n, where vector $x_i$ is the $i^{th}$ sample of input vector **x**, $y_i$ is the $i^{th}$ target value corresponding to $x_i$, n is the number of samples. First, SVR defines a nonlinear mapping $\Phi$, as shown in Eq.(3), to map input vector **x** into a high dimensional feature space. In the feature space, SVR aims to find a linear function *f(z)* to make the deviation between the calculated targets and the actual targets within the predefined tolerance. *f(z)* can be described as Eq.(4). In order to determine the coefficient vector ω, SVR minimize the overall training error as shown in Eq.(5) with the constraints in Eq.(6). During the solution of the optimization problem, a kennel function $k(x_i,x_j)=\varphi(x_i)^{T}\varphi(x_j)$ would be introduced.

$$\Phi : z = \varphi(x) \quad (3)$$

$$f(z) = \omega^{T} z + b \quad (4)$$

$$\text{minimize } \frac{1}{2}\omega^T\omega + C\sum_{i=1}^{n}(\xi_i + \xi_i^*) \tag{5}$$

$$\text{subject to } \begin{cases} y_i\text{-}(\omega^T z + b) \le \varepsilon + \xi_i \\ (\omega^T z + b)\text{-}y_i \le \varepsilon + \xi_i^*, \\ \xi_i, \xi_i^* \ge 0 \end{cases} \tag{6}$$

Where, **x** is the input vector; $z$ is the mapped vector; ω and b are the coefficients to be determined; $\varepsilon$ is the maximum value of the tolerance; $\xi_i$ and $\xi^*_i$ represent the training error above and below $\varepsilon$ respectively; C>0 is the penalty parameter of the error terms in Eq.(5).

In this study, SVR is constructed using the MATLAB LIBSVM toolbox [33]. LibSVM is a library for support vector machines, which aims at promoting SVM or SVR as a convenient tool. It integrates C-SVM classification, nu-SVM classification, one-class- SVM, epsilon-SVM regression, and nu-SVM regression. The following steps were employed for implementing LIBSVM tool box in this study. First, 70 samples including the variables of Eq.(1), generated by the simulated chilled water system, were selected and transformed as the input data set for training in the LIBSVM. Then, different kernels were tried and the related parameters were optimized. The proper kernel function and the related optimized parameters, which could obtain the best prediction results, were employed. Last, the SVR model was tested and integrated into the test platform as a module for online predictions. It is noted that the specific form of expression for the global AHU model (i.e. Eq.(1)) would not be clearly presented due to the black-box nature of SVR, in which the input data is mapped implicitly to high-dimensional feature space.

### 3.4 Hydraulic water network model using adaptive concept

Based on the predicted water flow ($M^*_{w,AHUS}$), the hydraulic water network models are employed to estimate the accurate water network pressure drop at the secondary side of heat exchangers, as shown in Fig.6. Considering the fact that there is normally no water flow meter for each AHU in most of the practical projects, the water flow rate of each AHU is not the necessary input in this study. Our work is to estimate the overall water resistance of the loop under each time step. The pressure drop of the loop then can be calculated using the

predicted overall water flow rate and the overall water resistance. Adaptive concept, which means the automatic adjustment of model parameters in real time during the control process, is introduced to accurately identify the current water resistance of the loop.

The loop through the remote terminal AHU is selected to establish this model. The total pressure drop ($PD^*_{tot,ahx}$) across this loop includes the pressure drop ($PD^*_{pf,tot,ahx}$) on the fittings around pumps (i.e. between points E and F), the pressure drop ($PD^*_{pipe,tot,ahx}$) on pipelines (i.e., the pipeline sections of D-E, F-$A_1$, $A_1$-$A_n$ and $B_n$-C) and the pressure drop ($PD^*_{term}$) on the remote terminal loop (i.e. $A_n$-$B_n$), as expressed in Eq. (7). Since the pressure drop of the heat exchanger group is overcome by the associated primary constant speed pumps, it is not included in this model. The pressure drop on the fittings around pumps can be calculated using Eq. (8). The first part at the right side of Eq. (8) calculates the water resistance of the overall pump group using the water resistance of individual pump fitting ($S_{pf,ahx}$) and the measured operating number of pumps ($N_{pu,sec,ahx}$). $S_{pf,ahx}$ needs to be identified before in-situ implementations. $S_{pf,ahx}$ can be considered as a constant that can be determined by measuring the pressure drop on single secondary pump after heat exchangers (i.e., pressure drop between points E and F in Figure 6) and its water flow rate.

The predicted benchmark of pressure drop of pipelines ($PD^*_{pipe,tot,ahx}$) can be calculated using Eq. (9). $S^k_{pipe,fic}$ represents a combined fictitious water resistance of all the pipelines of the loop at time step $k$. Ideally, $S^k_{pipe,fic}$ in Eq.(9) can be expressed as Eq.(10), which is deduced by three equations: Eq.(11)-(13). It can be observed that $S^k_{pipe,fic}$ reflects the dynamic water flow through each AHU ($M^k_{A,i}$) as a percentage of the total water flow rate ($M^k_{w,AHUs}$). Because there is normally no water flow meter installed for each AHU in real applications, $S^k_{pipe,fic}$ cannot be calculated directly using Eq.(10). Therefore, in this study, an adaptive concept is introduced, which aims to online automatically update and tune the parameters to enhance the accuracy of prediction models. At time $k$, $S^k_{pipe,fic}$ can be determined in Eq.(14) by using the measured pump head ($H^k_{pu,sec,ahx}$), the measured total water flow rate ($M^k_{w,AHUs}$) and the measured pressure drop ($PD^k_{term}$) of the remote terminal loop. $M^k_{w,AHUs}$ can be measured by a flow meter installed on the main pipe. $PD^k_{term}$ can be measured by a pressure meter installed across the remote terminal loop.

$$PD^{*}_{tot,ahx} = PD^{*}_{pf,tot,ahx} + PD^{*}_{pipe,tot,ahx} + PD^{*}_{term} \quad (7)$$

$$PD^{*}_{pf,tot,ahx} = (S_{pf,ahx} / N^{2}_{pu,\sec,ahx})(M^{*}_{w,AHUs})^{2} \quad (8)$$

$$PD^{*}_{pipe,tot,ahx} = S^{k}_{pipe,fic}(M^{*}_{w,AHUs})^{2} \quad (9)$$

$$S^{k}_{pipe,fic} = S_1 + S_2 + S_3 + \sum_{i=1}^{n-1} S_{A,i}(M^{k}_{A,i} / M^{k}_{w,AHUs})^{2} \quad (10)$$

$$PD^{k}_{pipe,tot,ahx} = (S_1 + S_2 + S_3)(M^{k}_{w,AHUs})^{2} + \sum_{i=1}^{n-1} S_{A,i}(M^{k}_{A,i})^{2} \quad (11)$$

$$PD^{k}_{pipe,tot,ahx} = (S_1 + S_2 + S_3)(M^{k}_{w,AHUs})^{2} + \sum_{i=1}^{n-1} S_{A,i}\frac{(M^{k}_{A,i})^{2}}{(M^{k}_{w,AHUs})^{2}}(M^{k}_{w,AHUs})^{2} \quad (12)$$

$$PD^{k}_{pipe,tot,ahx} = S^{k}_{pipe,fic}(M^{k}_{w,AHUs})^{2} \quad (13)$$

$$S^{k}_{pipe,fic} = [H^{k}_{pu,sec,ahx} - S_{pf,ahx}(M^{k}_{w,AHUs})^{2} / N^{2}_{pu,sec,ahx} - PD^{k}_{term}]/(M^{k}_{w,AHUs})^{2} \quad (14)$$

where, $S_1, S_2, S_3, S_{A,1} \ldots S_{A,n-1}$ are water resistances of various pipeline sections.The structure of the water network before heat exchangers can be regarded as the simplification of that after heat exchangers. Therefore, the model for water network before heat exchangers is not given in detail.

### 3.5 Pressure drop model for the remote terminal loop using adaptive concept

The model of pressure drop of the remote terminal loop is developed to predict the benchmark of the pressure drop ($PD^{*}_{term}$) on the remote AHU loop. In this study, the pump speed is controlled to maintain the pressure drop ($PD_{term}$) of the remote terminal loop at a variable set-point to always keep its valve nearly fully open. $PD_{term}$ (i.e. the pressure drop on $A_n$-$B_n$ in Fig. 6) can be calculated using the water resistance of this loop and the water flow rate through this AHU, as shown in Eq. (15). The water resistance of the remote terminal loop (i.e. $S_{term}$) is the combination of the water resistance of the cooling coil, the modulating valve, and the associated pipeline. Eq. (15) can be re-written as Eq. (16) by introducing the predicted total water flow rate ($M^{*}_{w,AHUS}$) of the zone. $S_{term,fic}$ ,which can be expressed as Eq. (17), represents the fictitious water resistance of the remote terminal loop. Since there is no flow meter for measuring the water flow of the terminal loop, $S_{term,fic}$ cannot be calculated by Eq. (17).

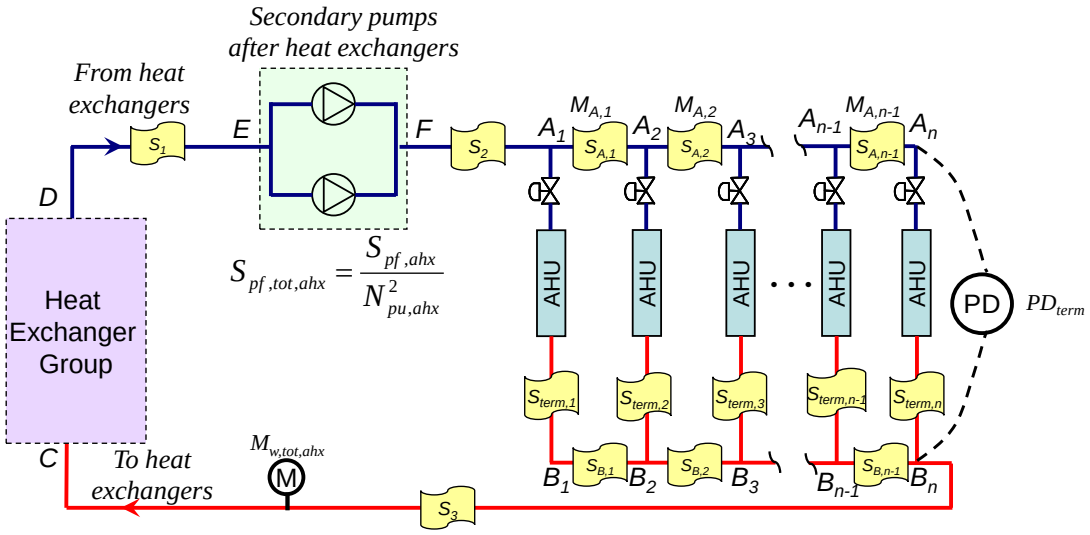


Fig. 6 Illustration of the hydraulic model of water network after heat exchangers

In this study, the adaptive concept is introduced to identify the current water resistance of the remote loop. At time step *k*, the current $S^{k}_{term,fic}$ can be determined by Eq.(18) using the measured pressure drop of the remote terminal loop by a pressure meter and the measured total water flow rate of the zone. The benchmark ($PD^{*}_{term}$) of the pressure drop of the remote terminal loop at time step *k* then can be calculated using Eq.(19) based on the predicted total water flow rate ($M^{*}_{w,AHUs}$).

$$PD_{term} = S_{term} M^{2}_{term} \tag{15}$$

$$PD_{term} = S_{term,fic} M^{2}_{w,AHUs} \tag{16}$$

$$S_{term,fic} = S_{term} (M_{term} / M_{w,AHUs})^{2} \tag{17}$$

$$S^{k}_{term,fic} = PD^{k}_{term} / (M^{k}_{w,AHUs})^{2} \tag{18}$$

$$PD^{*}_{term} = S^{k}_{term,fic} (M^{*}_{w,AHUs})^{2} \tag{19}$$

### 3.6 Plate heat exchanger model

The model of heat exchangers is used to predict the required water flow rate at the primary side of the heat exchangers ($M^{*}_{w,tot,bhx}$). The input data of this model are the measured cooling load ($Q_{AHUs}$), the water flow rate of all AHUs ($M^{*}_{w,AHUs}$), the required operating number of heat exchangers ($N_{hx}$), and the inlet water temperature at the primary side of heat exchangers ($T_{in,bhx}$).

This model is developed using the *ε-NTU* method based on the basic principle of

thermodynamics. Equations (20)-(23), which are common in many textbooks and handbooks, are employed to show how to predict the chilled water flow rate at the primary side of individual heat exchanger. First, in Eq.(20), the conductance-area product (*UA*) can be calculated which considers the effect of water flow on both sides of heat exchangers. Then, using Eq.(21) and (22), the overall number of transfer units (*NTU*) and the heat transfer effectiveness (ε) can be calculated. Eq. (23) shows the calculation of cooling load. By solving Eq.(20)-(23), the water flow rate at primary side of individual active heat exchanger($M_{w,bhx}$) can be determined. Correspondingly, the benchmark of the water flow rate ($M^*_{w,tot,bhx}$) of the primary side of all active heat exchangers

$$UA = UA_{des}(M_{w,bhx})^{b_0}(M_{w,ahx})^{b_1} \tag{20}$$

$$NTU = \frac{UA}{C_{\min}} \tag{21}$$

$$\varepsilon = \frac{1-\exp(-NTU(1-\frac{C_{\min}}{C_{\max}}))}{1-\frac{C_{\min}}{C_{\max}}\exp(-NTU(1-\frac{C_{\min}}{C_{\max}})} \tag{22}$$

$$Q_{AHUs} = \varepsilon \cdot C_{\min}(T_{in,ahx} - T_{in,bhx}) \tag{23}$$

$$M^*_{w,tot,bhx} = M_{w,bhx} N_{hx} \tag{24}$$

where, *UA* is the conductance-area product; $UA_{des}$ is the design value of *UA*; $M_{w,bhx}$ is the water flow rate at the primary side of individual heat exchanger; $M_{w,ahx}$ is the water flow rate at the secondary side of individual heat exchanger; *NTU* is the overall number of transfer units; ε is the heat transfer effectiveness; $T_{in,bhx}$ is the inlet water temperature at primary side of heat exchanger; $T_{in,ahx}$ is the inlet water temperature at secondary side of heat exchanger; *C* is the mass flow rate capacity; $N_{hx}$ is required number of heat exchangers in operating.

It is noted that the used input data of $T_{in,bhx}$ is the predefined set-point of chiller supply water temperature instead of the measured value.

### 3.7 Pump model

The pump model is used to predict the energy consumption of pumps when the total water flow rate through pumps and the pump head are known. In this study, the performance of variable speed pumps are modeled using a series of polynomial approximations based on the

references [34], including polynomials representing head versus flow and speed, and efficiency versus flow and speed.

Eq. (25) describes the pumps head ($H_{pu}$) as a function of the water flow rate ($M_w$) and the operating frequency (*Fre*). Eq. (26) is used to calculate the power input to a pump-motor-VFD set with given the pumps efficiency ($\eta_{pu}$), motor efficiency ($\eta_m$), and variable frequency drive efficiency ($\eta_v$). The efficiencies of pump, motor and VFD can be described as in Eq. (27), Eq. (28), and Eq. (29) respectively.

$$H_{pu} = c_0 M_w^2 + c_1 M_w Fre + c_2 Fre^2 \tag{25}$$

$$P_{pu} = M_w H_{pu} / (1000 \eta_{pu} \eta_{vfd} \eta_m) \tag{26}$$

$$\eta_{pu} = d_0 + d_1 M_w Fre + d_2 M_w^2 Fre^2 \tag{27}$$

$$\eta_m = e_0 (1 - e^{e_1 Fre}) \tag{28}$$

$$\eta_{vfd} = f_0 + f_1 Fre + f_2 Fre^2 + f_3 Fre^3 \tag{29}$$

### 3.8 Determination of operating number of heat exchangers and pumps

It is essential to accurately predict the required operating number of heat exchangers and pumps because the operating numbers significantly affect the pump energy. In this method, the determinations of the required operating number of heat exchangers and pumps are predicted based on the sequence control strategy of heat exchanger and pump adopted in this HVAC system studied.

For heat exchangers, the required operating number is reset to be twice as many as the operating number of secondary pumps after heat exchangers. For secondary variable speed pumps, an additional pump is switched on when the frequencies of operating pumps exceed 90% (corresponding to 45Hz) of their nominal capacity. One of the operating pumps is switched off when the frequencies of the operating pumps are lower than 60% (corresponding to 30Hz) of the nominal capacity. For primary constant speed pumps after heat exchangers, their operating number is the same as the operating number of the heat exchangers.

### 3.9 The detailed application procedures

The detailed application procedure is illustrated as below (the outline is illustrated earlier in Fig. 5). The required main measurements include the cooling load of the zone concerned, the indoor air temperature, the total water flow rate of the zone concerned, the head of pumps at both sides of heat exchangers and the pressure over the remote loop.

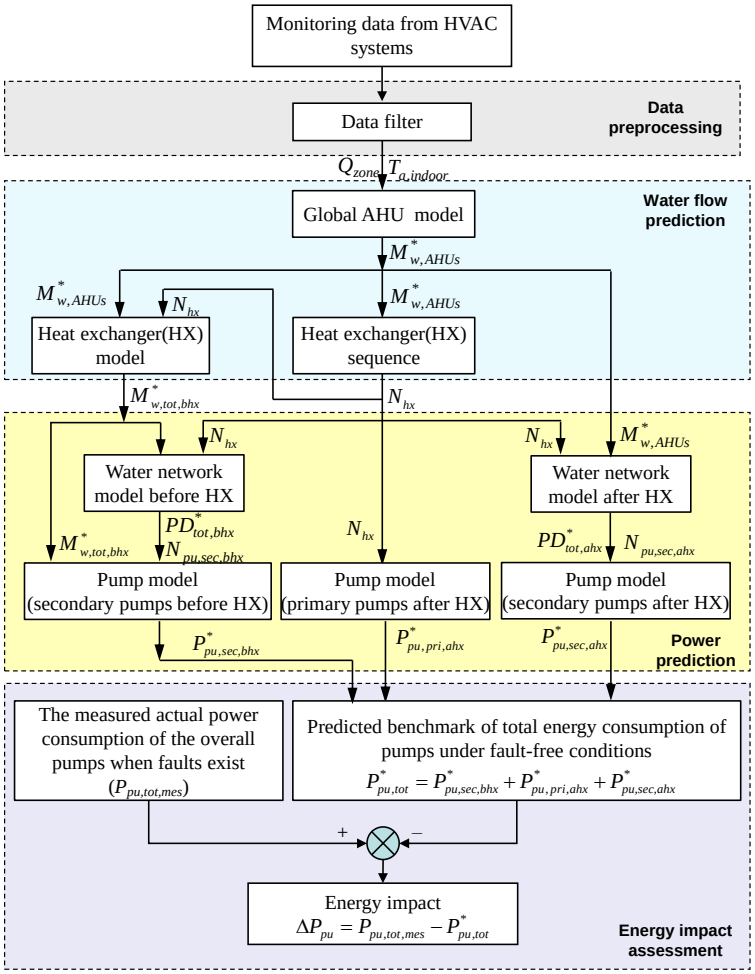


Fig. 5 Flow chart of the energy impact evaluation

(1) Check the measurements using a data preprocessor to eliminate unreasonable values;

(2) Calculate the benchmark of total water flow required in the zone using the global AHU model(Eq. (1) and (2));

(3) Determine the required operating number of heat exchangers based on the sequence control strategy used;

(4) Calculate the required water flow at the primary side of the heat exchangers using the heat exchanger model (Eq.(20) – (24));

(5) Calculate the pressure drop of the overall hydraulic water loop at the primary and

secondary the heat exchangers using the hydraulic water network model, respectively (Eq.(7),(8),(9), (14));

(6) Calculate the power of three group of pumps respectively, i.e. variable speed pumps at primary and secondary sides of heat exchangers, and constant speed pumps associated with heat exchangers (Eq.(25)-(29));

(7) Determine the energy impact of the overall pumps by comparing the measured power with the predicated benchmark.

## 4. Performance tests and evaluation

### 4.1 Setup of the test platform

The proposed method is validated and evaluated using a computer-based simulation platform that was established based on the detailed information of the actual complex chilled water system as in Fig. 2. This is a complex primary-secondary chilled water system. In the secondary loop, heat exchangers are used to transfer the cooling energy from chillers to terminal units. After each heat exchanger, a primary constant speed pump is installed to ensure the constant flow through each heat exchanger. The AHU valves are modulated to maintain the supply air temperature at its set-point (i.e.13℃). The AHU fans are equipped with variable speed drives to maintain the indoor air temperature at a fixed set-point (i.e.25℃). Chiller supply water temperature is maintained at 5.5℃. The entire simulation platform is developed using TRNSYS. The major components, such as the chillers, cooling towers, pumps, heat exchangers and cooling coils, are modeled using detailed physical models. The weather data used is the data of the typical year in Hong Kong.

### 4.2 Validation of the individual models developed

The developed predictive models were tested respectively on the test platform under various operating cooling load ratios of the entire system concerned. The “measured” fault-free operation data produced by the test platform were used to train the models. Fig. 7 shows the results by comparing the “measured” values collected from the test platform with those predicted by the models.

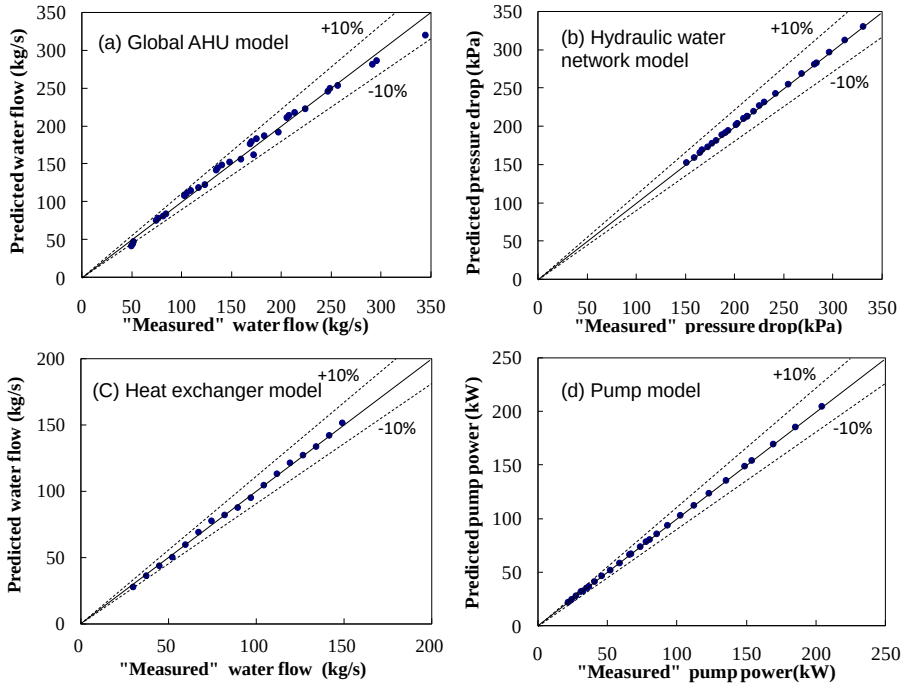


Fig. 7 Validation of individual predictive models

When validating the global AHU model, different combinations of AHUs with different load ratios were tested under one certain system cooling load. It can be found in Fig. 7(a) that most of the points, particularly under the cooling load ratios not less than 20%, are located in the range with the relative error of 10%. The relative errors became larger under the cooling load ratios below 20%. This is because the performance of cooling coils will change extremely nonlinearly under low load ratios due to the laminar flow. For the heat exchanger model, the maximum relative error is 6%, occurring under low water flow rate. The maximum relative error for the pump model and hydraulic water network model is 2.1% and 1.5%, respectively. The validation results mean these models have good performances in prediction.

### 4.3 Validation of the entire predictive method for energy benchmark

The proposed whole predictive method for predicting energy benchmark, consisting of the developed predictive models, is also tested on the simulation platform under three typical weather conditions, representing the chilled water system working under spring, mild-summer and sunny-summer days. During the tests, there are no faults in the system and the operating parameters are maintained at the preset values, including the supply air

temperature (13°C), the supply water temperature set-point after heat exchangers (6.3°C), and the supply water temperature set-point before heat exchangers (5.5°C). Based on the measured cooling load and the preset set-points above, the proposed method predicted the water flow rate demanded by all the terminal units and the pump energy consumption.

As examples, Table 3 summarizes the results under three typical cooling load conditions, which compares the prediction results using the proposed method (predicted values) with the results measured from the simulation platform ("measured" values). It can be observed that the total power consumptions of pumps predicted by the proposed method agreed well with that the "measured" values under the three working conditions. The maximum relative difference between the two methods was only about 2.74%. The operating numbers of pumps and heat exchangers predicted by the proposed method were also the same as those in the ideal tests.

Table 3 Comparison between performance data using the proposed method and in the idea tests

| | Seasons | | | | | |
|---|---|---|---|---|---|---|
| | Spring | | Mild-summer | | Sunny-summer | |
| *Typical working conditions* | | | | | | |
| Cooling load (kW) | 4646.48 | | 7350.88 | | 10149.52 | |
| Chiller operating number | 1 | | 2 | | 2 | |
| Chiller supply water temperature (°C) | 5.50 | | 5.50 | | 5.50 | |
| | Comparisons | | | | | |
| | Predicted results | "Measured" results | Predicted results | "Measured" results | Predicted results | "Measured" results |
| $M_{w,AHUs}$ (l/s) | 170.89 | 166.76 | 301.62 | 300.76 | 461.32 | 465.08 |
| $N_{pu,sec,bhx}$ | 1 | 1 | 1 | 1 | 2 | 2 |
| $N_{pu,sec,ahx}$ | 1 | 1 | 2 | 2 | 2 | 2 |
| $N_{pu,pri,ahx}$ | 2 | 2 | 3 | 3 | 4 | 4 |
| $N_{hx}$ | 2 | 2 | 3 | 3 | 4 | 4 |
| $P_{pu,sec,bhx}$ (kW) | 15.6 | 14.82 | 61.99 | 60.79 | 85.06 | 88.47 |
| $P_{pu,sec,ahx}$ (kW) | 40.48 | 37.38 | 83.08 | 79.55 | 168.44 | 172.29 |
| $P_{pu,p,iahx}$ (kW) | 89.4 | 89.4 | 134.1 | 134.1 | 178.8 | 178.8 |
| *Total* (kW) | 145.48 | 141.6 | 279.17 | 274.44 | 432.3 | 439.56 |
| Deviation*(kW) | 3.88 (2.74%) | - | 4.73 (1.72%) | - | -7.26 (-1.65%) | - |

*Value in parentheses indicates the percentage of the prediction deviates from the "measurements"

### 4.4 Case study: Energy impact evaluation using the proposed method

The proposed method is used to evaluate the energy impact of pumps when the low delta-T syndrome exists in the chilled water system. The tests are conducted on the simulated

platform in three days between 8:00am to 18:00pm under typical spring, mild summer and sunny summer weather conditions respectively. The cooling load profiles of the three weather days are shown in Fig. 8.

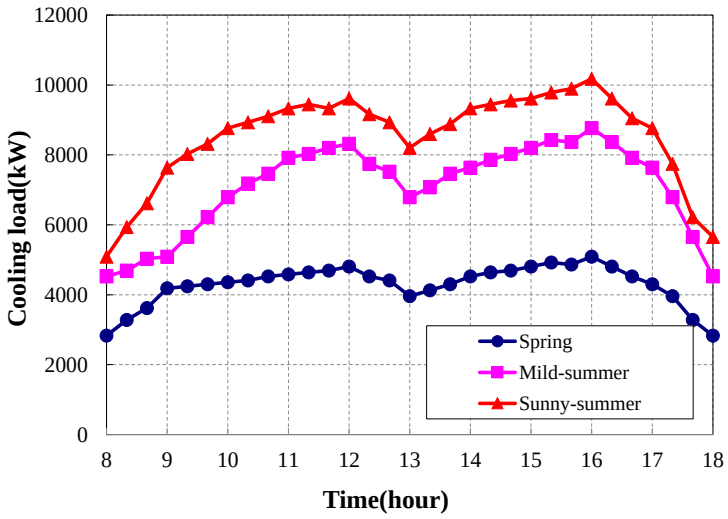


Fig. 8 Cooling load profile of three weather days

*4.4.1 Faults introduction*

During the tests, two typical faults, the performance degradations of AHU coils and plate heat exchangers, are introduced artificially as the example faults causing the low delta-T syndrome. When the performance of the cooling coil is degraded, such as coil fouling, the heat transfer effect between the inlet air and inlet water is significantly decreased. More chilled water is required and the water temperature difference produced by the coil is decreased when handling the same cooling load.

Cooling coils degradation in AHU is introduced by increasing the thermal resistance at water side artificially by two levels respectively (i.e., water thermal resistance is increased by 40% and 80%). Performance degradation of plate heat exchangers is introduced by reducing the overall conductance–area product ($UA_{HX}$) artificially in two quantities (i.e., $UA_{HX}$ is reduced by 20% and 30%) respectively.

*4.4.2 Results analysis*

Figures 9-11 compare the total pump energy consumptions under different fault levels in the

typical spring, mild-summer and sunny-summer days respectively. The power consumption predicted by the proposed method is used as the benchmark for comparison. It is obvious that significant energy of pumps were wasted when performances of AHUs and heat exchangers were degraded. More energy was consumed when the faulty severity level was increased. It also can be found that the faults of AHU degradation had more effect on the energy consumption than the faults of heat exchanger degradation.

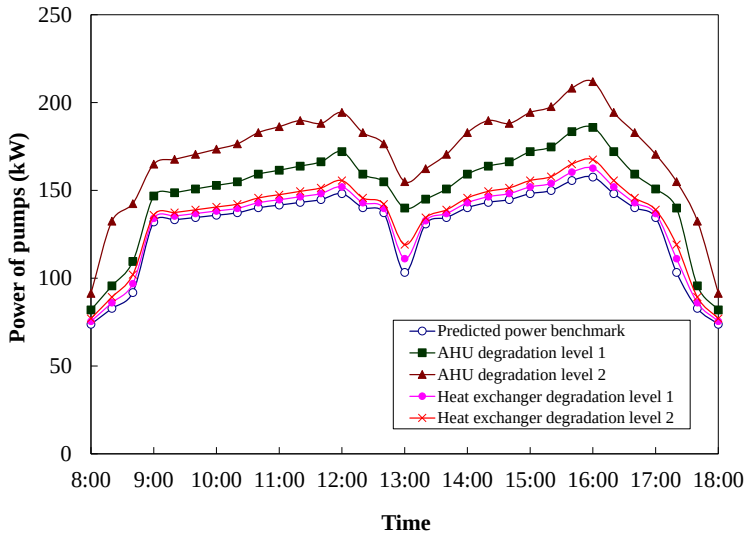


Fig. 9 Power consumptions of pumps in the Spring test case

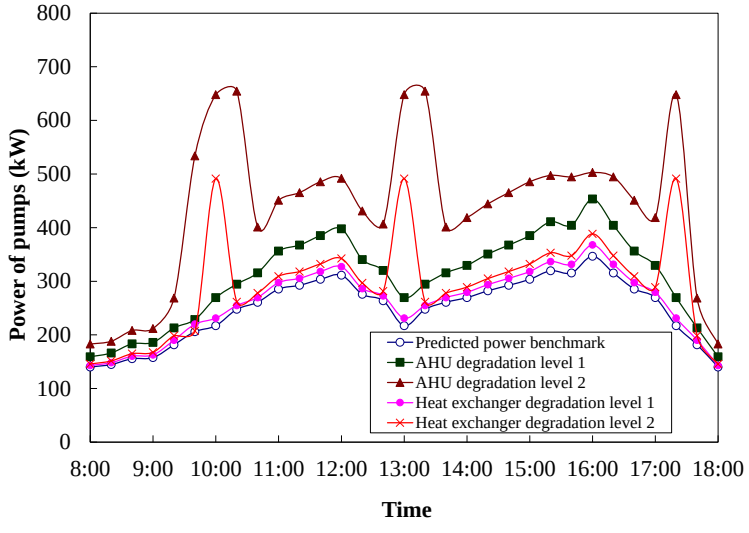


Fig. 10 Power consumptions of pumps in the Mild-Summer test case

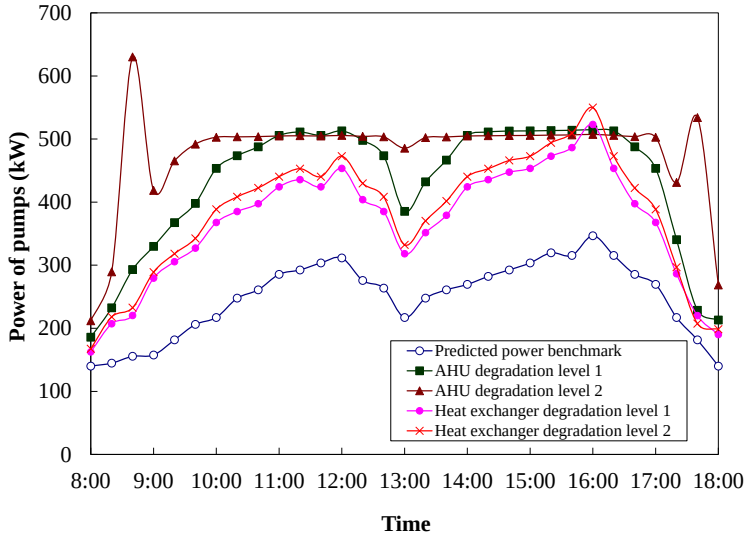


Fig. 11 Power consumptions of pumps in the Sunny-Summer test case

It is worthy noticing that there were several sudden increases of pump power with the faults of "AHU degradation level 2" and "heat exchanger degradation level 2" in the mild-summer and sunny-summer test cases, such as the points near 10:00, 13:00 and 17:20 in Fig. 10 as well as the points near 8:40 and 17:40 in Fig.11. In particular, although the cooling load of 13:00 in the mild-summer case was lower than the others, the pump energy use was extremely high. The reason is that the deficit flow was triggered under those points. The reason is that the deficit flow was triggered under those working points. Actually, the deficit flow does not always occur even the system is degraded by serious water fouling. It is more easily triggered when the water flow rate of the secondary loop (before heat exchangers) approaches that of the primary loop. At these moments, due to the faults (e.g. coil fouling), extra water was required in order to maintain the supply water temperature after heat exchangers maintained at the set-point. That would result in the fact that the water flow rate of secondary loop exceeds that of the primary loop. The deficit flow was triggered and in turn increased the supply water temperature before heat exchangers, which further made the supply water temperature after heat exchangers hard to achieve the set-point. When the serious vicious circle occurred, the pumps before heat exchangers were continuously speeded and largely deviated from the normal conditions. Therefore, extreme more pump energy was consumed.

Table 4 summaries the daily (between 8:00am and 18:00pm) energy impacts of pumps under different faults levels in the three typical days. The maximum energy impact of pumps occurred in the mild-summer test case when the AHU degradation was increased to Level 2. About 75.22% of the total pumps energy was wasted when comparing to the reference benchmark. It is also showed that the energy impact resulted from heat exchanger degradation was mainly contributed by the secondary pumps before heat exchangers. The energy impact due to AHU degradation was mainly contributed by the secondary pumps after heat exchangers particularly under low fault level.

Table 4 Daily energy consumption of pumps under different faults levels in three typical days

| Strategies | $P_{pu,sec,bhx}$ (kWh) | $P_{pu,pri,ahx}$ (kWh) | $P_{pu,sec,ahx}$ (kWh) | Total (kWh) | $P_{pu,sec,bhx}$ impact (kWh) | (%) | $P_{pu,pri,ahx}$ impact (kWh) | (%) | $P_{pu,sec,ahx}$ impact (kWh) | (%) | Total impact (kWh) | (%) |
|---|---|---|---|---|---|---|---|---|---|---|---|---|
| Spring | | | | | | | | | | | | |
| Predicted benchmark | 152.58 | 819.50 | 363.66 | 1335.74 | - | - | - | - | - | - | - | - |
| AHU degradation | | | | | | | | | | | | |
| Level 1 | 219.34 | 849.30 | 471.00 | 1539.64 | 66.76 | 43.75 | 29.8 | 3.64 | 107.34 | 29.52 | 203.9 | 15.26 |
| Level 2 | 292.00 | 894.00 | 583.26 | 1769.26 | 139.42 | 91.38 | 74.5 | 9.09 | 219.6 | 60.39 | 433.52 | 32.46 |
| Heat exchanger degradation | | | | | | | | | | | | |
| Level 1 | 187.27 | 819.50 | 363.66 | 1370.43 | 34.69 | 22.74 | 0 | 0 | 0 | 0 | 34.69 | 2.60 |
| Level 2 | 220.77 | 819.50 | 363.67 | 1403.94 | 68.19 | 44.69 | 0 | 0 | 0 | 0 | 68.2 | 5.11 |
| Mild-summer | | | | | | | | | | | | |
| Predicted benchmark | 449.75 | 1221.80 | 897.80 | 2569.35 | - | - | - | - | - | - | - | - |
| AHU degradation | | | | | | | | | | | | |
| Level 1 | 648.99 | 1235.63 | 1281.40 | 3166.02 | 199.24 | 44.30 | 13.83 | 1.13 | 383.6 | 42.73 | 596.67 | 23.22 |
| Level 2 | 1116.01 | 1653.90 | 1732.01 | 4501.92 | 666.26 | 148.14 | 432.1 | 35.37 | 834.21 | 92.92 | 1932.57 | 75.22 |
| Heat exchanger degradation | | | | | | | | | | | | |
| level 1 | 563.45 | 1221.80 | 897.80 | 2683.05 | 113.7 | 25.28 | 0 | 0 | 0 | 0 | 113.7 | 4.43 |
| level 2 | 839.19 | 1266.50 | 926.04 | 3031.73 | 389.44 | 86.59 | 44.7 | 3.66 | 28.24 | 3.15 | 462.38 | 18.00 |
| Sunny-summer | | | | | | | | | | | | |
| Predicted benchmark | 747.97 | 1490 | 1379.40 | 3617.38 | - | - | - | - | - | - | - | - |
| AHU degradation | | | | | | | | | | | | |
| Level 1 | 970.39 | 1624.10 | 1849.63 | 4444.12 | 222.42 | 29.74 | 134.1 | 9.00 | 470.23 | 34.09 | 826.74 | 22.85 |
| Level 2 | 1103.02 | 1773.10 | 2065.30 | 4941.42 | 355.05 | 47.47 | 283.1 | 19.00 | 685.9 | 49.72 | 1324.04 | 36.60 |
| Heat exchanger degradation | | | | | | | | | | | | |
| Level 1 | 926.01 | 1490.00 | 1379.40 | 3795.41 | 178.04 | 23.80 | 0 | 0 | 0 | 0 | 178.03 | 4.92 |
| Level 2 | 1099.96 | 1490.00 | 1379.41 | 3969.37 | 351.99 | 47.06 | 0 | 0 | 0 | 0 | 351.99 | 9.73 |

Accordingly, the system temperature difference at primary side of heat exchanger group (i.e., *ΔT1*) and the system temperature difference of the overall AHUs (i.e., *ΔT2*) are presented in Fig. 12 and 13. The results are from the mild-summer case, as the example, to illustrate the severity of the low delta-T syndrome under different faults. For *ΔT1*, compared with the benchmark, the temperature difference was highly reduced under both AHU fouling and heat

exchanger fouling. There are some points, whose temperature difference is extremely lower than the benchmark, such as the points near 10:00, 13:00 and 17:20. This is because the oversupplied water at primary side of heat exchanger triggered the deficit flow, which has been discussed earlier.

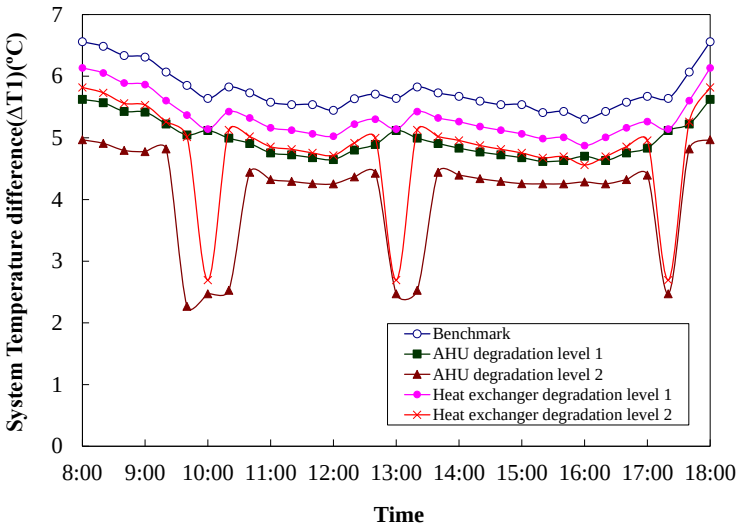


Fig. 12 System tempreatrue difference at primary side of heat exchangers (ΔT1)

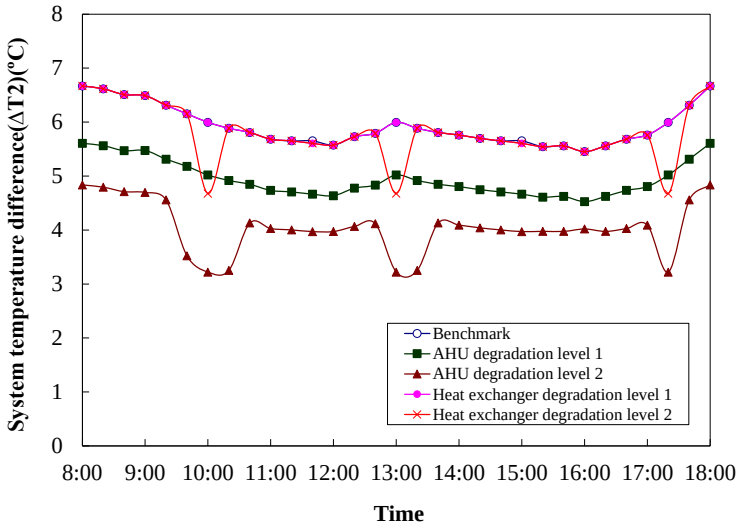


Fig. 13 System tempreatrue difference of overall AHUs (ΔT2)

For *ΔT2*, it can be observed that AHU fouling could result in significant lowered temperature difference because more water is required by AHUs to maintain the supply air temperature at the same set-point when coils become fouled. It also can be found that heat exchanger fouling

almost has no effect on *ΔT2*. During most of the time, the temperature difference under heat exchanger fouling maintained the same as the benchmark. There are only several points, at which the temperature difference highly deviate from the benchmark. The reason is also the deficit flow at primary side of heat exchangers. When the deficit flow occurred, the supplied water temperature to the AHUs cannot could be higher than the predefined set-point. More water thus is required by AHUs, which results in the lowered temperature difference of AHUs.

It is worthy noticing that the system temperature differences (*ΔT1* and *ΔT2*) still maintained over 5ºC at many points even there exist the AHU coil fouling or heat exchanger fouling. The reason is the nature of a variable water flow system, in which the design differential temperature (e.g. 5 ºC) can be achieved under full load conditions. While under part load conditions, the temperature difference could be significantly higher than the design value because the heat transfer areas almost maintain unchanged.

## 5. Conclusions

A model-based method is developed for evaluating the energy impact on the chilled water pumps due to the low delta-T syndrome in complex chilled water systems. SVR method is employed to accurately predict the benchmark of the system water flow rate considering the load ratio of individual AHUs. Adaptive concept is introduced to identify the water resistance for accurate prediction of pump head. This method was tested and validated in a dynamic simulation platform representing a real complex HVAC system. The results show that the proposed energy impact evaluation method can accurately predict the reference benchmark of chilled water pump energy under various working conditions. The energy impact of pumps therefore can be determined by comparing the measured pump energy with the reference benchmark when the low delta-T syndrome occurs.

This method is applicable in the real chilled water system for diagnosing and quantitatively evaluating the energy impact due to the low delta-T syndrome. The evaluation results are the useful references for operators on whether taking measures to correct the faults and improve the energy performance of the chilled water distribution system.

## Acknowledgements

The research presented in this paper is financially supported by a grant (5276/12E) of the Research Grant Council (RGC) of the Hong Kong SAR. The authors would like to acknowledge the support of Sun Hung Kai Real Properties Limited and the Research Institute of Sustainable Urban Development (RISUD) of The Hong Kong Polytechnic University.

## References

1 U.S. Department of Energy. *Building energy data book* 2010.
2 JJ Wang, YY Jing, CF Zhang. Fuzzy multi-criteria evaluation model of HVAC schemes in optimal combination weighting method. *Building Services Engineering Research and Technology* 2009; 30(4): 287–304.
3 Xiwang Li, Wen Jin. Building energy consumption on-line forecasting using physics based system identification. *Energy and Buildings* 2014; 82: 1–12.
4 Shun Li, Jin Wen. A model-based fault detection and diagnostic methodology based on PCA method and wavelet transform. *Energy and Buildings* 2014; 68: 63–71.
5 ZJ Ma, SW Wang. Test and evaluation of energy saving potentials in a complex building central chilling system using genetic algorithm. *Building Services Engineering Research and Technology* 2011; 32(2): 109–126.
6 Xuemin Sui, Xu Zhang, and Xing Han, Performance analysis on a residential radiant chilled ceiling system and evaluation on indoor thermal environment in summer: an application. *Building Services Engineering Research and Technology* 2013; 34(3): 317–331.
7 Yongjun Sun, Pei Huang, Gongsheng Huang. A multi-criteria system design optimization for net zero energy buildings under uncertainties. *Energy and Buildings* 2015; 97: 196–204.
8 Pei Huang, Gongsheng Huang, Yu Wang. HVAC system design under peak load prediction uncertainty using multiple-criterion decision making technique. *Energy and Buildings* 2015; 91: 26–36.
9 Natasa Djuric, Vojislav Novakovic. Identifying important variables of energy use in low energy office building by using multivariate analysis. *Energy and Buildings* 2012; 45: 91–98.
10 Qiuyuan Zhu, Xinhua Xu, Jiajia Gao, Fu Xiao. A semi-dynamic model of active pipe-embedded building envelope for thermal performance evaluation. *International Journal of Thermal Sciences* 2015; 88: 170-179.
11 W. Kirsner. Demise of the primary-secondary pumping paradigm for chilled water plant design. *HPAC Engineering* 1996; 68(11): 73–78.
12 J.P. Waltz. Variable flow chilled water or how I learned to love my VFD. Energy Engineering 2000; 97(6): 5–32.
13 W. Kirsner. Rectifying the primary-secondary paradigm for chilled water plant design to deal with low ΔT central plant syndrome. *HPAC Engineering* 1998; 70(1): 128–131.
14 G. Avery. Controlling chillers in variable flow systems. ASHRAE Journal 1998; 40(2): 42–45.
15 McQuay. *Chiller Plant Design: Application Guide AG 31-003-1*. McQuay International, 2002.
16 S.T. Taylor. Degrading chilled water plant delta-T: causes and mitigation. *ASHRAE Transaction* 2002; 108 (1): 641–653.
17 T.H. Durkin. Evolving design of chiller plants. *ASHRAE Journal* 2005; 47(11): 40–50.
18 DC Gao, SW Wang, YJ Sun, F Xiao. Diagnosis of the low temperature difference syndrome in the chilled water system of a super high-rise building: A case study. *Applied Energy* 2012; 98: 597–606.
19 D.P. Fiorino. Achieving high chilled-water delta Ts. *ASHRAE Journal* 1999; 41: 24–30.
20 G. Avery. Improving the efficiency of chilled water plants. ASHRAE Journal 2001; 43(5): 14–18.
21 D. P. Fiorino. How to Raise Chilled Water Temperature Differentials. *ASHRAE Transactions* 2002;

108 (1): 659–665.
22 DC Gao, SW Wang, YJ Sun. A fault-tolerant and energy efficient control strategy for primary–secondary chilled water systems in buildings. Energy and buildings 2011; 43(12): 3646–3656.
23 SW Wang, ZJ Ma, DC Gao. Performance enhancement of a complex chilled water system using a check valve: Experimental validations. *Applied Thermal Engineerin*g 2010; 30: 2827–2832.
24 ZJ Ma, SW Wang, WK Pau, Secondary loop chilled water in super high-rise. *ASHRAE Journal* 2008, 50(5): 42-52.
25 ZJ Ma, SW Wang. Supervisory and optimal control of central chiller plants using simplified adaptive models and genetic algorithm. *Applied Energy* 2011; 88: 198–211.
26 ZJ Ma, SW Wang. An optimal control strategy for complex building central chilled water systems for practical and real-time applications. *Building and Environment* 2009; 44: 1188–1198.
27 VN Vapnik. *Statistical Learning Theory*. Wiley, New York, 1998.
28 VN Vapnik. *The Nature of Statistical Learning Theory*. Springer, New York, 2000.
29 Xue-Cheng Xi, Aun-Neow Poo, Siaw-Kiang Chou. Support vector regression model predictive control on a HVAC plant. Control Engineering Practice 2007; 15(8): 897-908.
30 Rishee K. Jain, Kevin M. Smith, Patricia J. Culligan, John E. Taylor. Forecasting energy consumption of multi-family residential buildings using support vector regression: Investigating the impact of temporal and spatial monitoring granularity on performance accuracy. Applied Energy 2014; 123: 168-178.
31 Xue-Bin Yang, Xin-Qiao Jin, Zhi-Min Du, et al. A hybrid model-based fault detection strategy for air handling unit sensors. *Energy and Buildings* 2013; 57: 132-143.
32 Jinxing Che, Jianzhou Wang, Guangfu Wang. An adaptive fuzzy combination model based on self-organizing map and support vector regression for electric load forecasting. *Energy* 2012; 37(1): 657-664.
33 C.C. Chang, C.J. Lin. LIBSVM: a library for support vector machines. ACM Transactions on Intelligent Systems and Technology 2011; 2(3): 27.
34 ZJ Ma, SW Wang. Energy efficient control of variable speed pumps in complex building central air-conditioning systems. Energy and Buildings 2009; 41: 197–205.